Assessment of Seismic Responses on the Concrete Gravity Dam Subjected to the Geometrical Design Parameters Using Finite Element Approach

Tuswan Tuswan
Department of Naval Architecture, Universitas Diponegoro

Muhammad, Rafi
Department of Mechanical Engineering, Universitas Sebelas Maret

Aditya Rio Prabowo
Department of Mechanical Engineering, Universitas Sebelas Maret

Yaningsih, Indri
Department of Mechanical Engineering, Universitas Sebelas Maret

他

https://doi.org/10.5109/7236865

出版情報：Evergreen. 11 (3), pp.2217-2233, 2024-09. 九州大学グリーンテクノロジー研究教育センター
バージョン：

Assessment of Seismic Responses on the Concrete Gravity Dam Subjected to the Geometrical Design Parameters Using Finite Element Approach

Tuswan Tuswan[1], Rafi Muhammad[2], Aditya Rio Prabowo[2,*], Indri Yaningsih[2], Wibowo Wibowo[2], Teguh Muttaqie[3], Iwan Istanto[2,4]

[1]Department of Naval Architecture, Universitas Diponegoro, Semarang 50275, Indonesia

[2]Department of Mechanical Engineering, Universitas Sebelas Maret, Surakarta 57126, Indonesia

[3]Research Center for Testing Technology and Standards, National Research and Innovation Agency (BRIN), Tangerang 15314, Indonesia

[4]Department of Electro-Mechanical, Polytechnic Institute of Nuclear Technology, Yogyakarta 55281, Indonesia

*Authors to whom correspondence should be addressed:
E-mail: aditya@ft.uns.ac.id

(Received October 28, 2023: Revised June 2, 2024: Accepted June 21, 2024).

Abstract: Gravity dams serve as critical infrastructure for water storage, flood control, and energy generation. Ensuring their structural integrity under seismic loading is essential for safeguarding lives, property, and the environment against the catastrophic consequences of dam failure. This study discusses the seismic response of the concrete gravity dam that was given the earthquake and hydrostatic forces using ABAQUS, which was validated with the experimental result from Hai-tao et al. study. In this case, four main variables, such as mesh size, dam gradient, dam width, and earthquake's peak due to Koyna earthquake in Mumbai, India are evaluated to compare the response of the dam under seismic response. The result shows larger gradient can be used to reduce stress on the dam's neck, a larger gradient on the dam's neck can have a negative impact because the majority of stress is distributed on the bottom part of the dam. In addition, varying the width of the dam's structure offers a potential solution to decrease stress on its lower section. However, as the width increases, tensile damage tendencies shift towards the upstream face, which is unfavorable. This indicates a heightened risk of the dam's susceptibility to fracture during earthquakes.

Keywords: Gravity dam; ABAQUS; seismic loading; stress response.

1. Introduction

Modern manufacturer infrastructure must undergo various computations to prevent the structure from collapsing. The demands to be assessed before constructing the structure include how long the structure can withstand pressure, the design of the structure, the height of the structure, the material required, and other factors. The computation is required to keep the building from collapsing due to usage or external influences such as a natural catastrophe. Natural disasters, including geological, biological, and mechanical processes, are all around us. Earthquakes are one of the natural calamities that impact human lives and the infrastructure around us[1)]. Low-frequency, high-impact catastrophes such as earthquakes and tsunamis are unavoidable yet can result in significant human casualties. Natural catastrophes kill around 45,000 individuals worldwide per year, accounting for roughly 0.1% of global mortality during the previous decade[2)]. That is one of the reasons why the infrastructure around us, such as gravity dams, must be calculated to avoid the influence from increasing.

A gravity dam is a structure built across a stream or river that uses the weight of the material against the foundation to oppose the pressure of the water pushing against it[3)]. The function is to hold water and then use it to control flooding, store water, and generate electricity, which is a significant support for developing clean energy. The seismic behavior of concrete gravity dams has been a prominent area of research for many years, primarily due to concerns about dam safety during earthquakes[4,5)]. These high concrete gravity dams are considered critical infrastructures, and their failure due to seismic activity

could result in substantial loss of life and significant property damage[6].

The collapse of dams results in a catastrophic event marked by the sudden discharge of water, posing significant concerns both economically and in terms of fatalities[7,8]. The literature contains numerous instances of concrete dams experiencing varying degrees of damage from earthquakes, such as the Koyna gravity dam during the Koyna earthquake in 1967, the Hsinfengking dam during the China earthquake in 1962, and the Shih-Gang Dam during the Chi-Chi earthquake in 1999[9]. Therefore, it's crucial to thoroughly analyze their response to seismic activity and ensure their safety[10,11].

Assessing the seismic vulnerability of concrete gravity dams is a complex task. Researchers globally have utilized various numerical modeling[12,13] and experimental approaches [14,15] to study their seismic response, drawing insights from existing literature. Additionally, specialized software tools have been developed for evaluating the structural integrity of these dams, with many employing Finite Element Analysis (FEA)[16-18]. Researchers have explored the earthquake-induced damage response of concrete gravity dams, considering the interaction between the dam and reservoir. They have compared the solutions provided by the Westergaard and Lagrangian methods for dam-reservoir interaction and examined how varying the viscous damping ratio affects dam damage response[19]. Additionally, Omidi et al. evaluated the seismic cracking of concrete gravity dams using a plastic-damage model, considering different damping mechanism[20].

According to prior research, the gravity dam's acceleration reaction during the Koyna earthquake near the dam crest was lessened when the strain rate impact was taken into account[21]. The study found the acceleration and displacement response from seismic simulation, with variations of 0.4g, 0.6g, 0.7g, and 0.8g, using a gravity dam as the model and the Koyna earthquake. The purpose of the model's development was to ascertain how strain rate affected the gravity dam's peak fluctuation during an earthquake. Nevertheless, the aforementioned prior study did not address fluctuations in the dam's breadth and gradient.

While the previous study provided valuable insights into the behavior of gravity dams under seismic loading, it primarily focused on strain rate effects, leaving gaps in our understanding regarding the influence of dam geometry. By incorporating gradient and width variations into the analysis, this research aims to fill this gap and provide a more comprehensive understanding of the factors influencing dam response to earthquakes.

This study uses advanced finite element analysis techniques (ABAQUS software)[22] to consider a range of variables, including mesh size, dam gradient, dam width, and earthquake intensity. By simulating the historic Koyna earthquake of 1967, which serves as a representative seismic event, this research provides valuable insights into the seismic vulnerability of concrete gravity dams under realistic loading conditions.

Overall, this study represents a significant step forward in dam engineering and seismic risk assessment, offering actionable insights that can help mitigate the potential consequences of seismic events on critical infrastructure and ensure the long-term safety and resilience of concrete gravity dams.

2. Earthquake: engineering perspective

An earthquake is the shaking of the earth's surface resulting from a sudden release of energy in the earth's lithosphere that creates seismic waves[23]. Earthquakes can range in intensity from weak earthquakes that cannot be felt to those earthquakes that can destroy lots of structures and take human life. Earthquakes are natural disasters resulting in huge losses of lives and properties around them. Since there is no way to prevent earthquakes in our lives, the design of structures and industrial developments must follow the possible types of earthquakes[24]. Earthquakes can occur far from the land, and their effects appear as severe shaking to the infrastructure on land. On the other hand, earthquakes can occur just beneath industrial zones or nearby vital infrastructure such as gravity dams[23].

As the impact of earthquakes is huge, engineers have started to study and analyze the impact and prevention of earthquakes on structures, which is called earthquake engineering. It is an interdisciplinary branch of engineering that designs and analyzes structures with earthquakes in mind, such as buildings, bridges, and dams. This scientific field's objectives are protecting society and the environment from earthquakes by limiting the seismic risk to socio-economically acceptable levels[25]. Designing and ensuring that the structure can hold the forces caused by earthquakes does not necessarily have to be extremely strong and expensive[26]. It has to be properly designed to withstand earthquake damage while sustaining an acceptable level of damage while maintaining the cost of making the structure[27]. To ensure the structures' design can hold the earthquake forces, engineers conduct some assessments that are performed experimentally or analytically.

Experimental evaluations are tests typically conducted by placing a scaled structure model on a shake test table that simulates the earthquake. These experiments were first performed more than a century ago and recently have become possible to perform 1:1 scale on full structures[28]. Even though the experimental evaluation is easier to analyze, the cost of building the scaled structure and executing the shake test table is expensive. Engineers tend to use experimental tests for understanding the seismic behavior of structures, validating models, and verifying analysis methods[29]. Therefore, computational models and numerical procedures are more effective than experimental procedures.

The analytical or numerical assessment utilizes detailed structure modeling with structural analysis methods to better understand structures' earthquake performance. This method is based on structural dynamics, which covers the behavior of a structure subjected to dynamic loading, such as earthquakes. The first earthquake simulation was performed by statically applying horizontal inertia forces based on scaled peak ground acceleration (PGA) or the maximum ground acceleration that occurred during the earthquake events to a mathematical model of a structure[30]. Earthquake simulations on structures are used to define the damage that occurred on the structure, such as stress, displacement, and tensile damage on the structure, where the damage results are usually used to obtain earthquake loss estimation[31]. Earthquake loss estimation is usually defined as Damage Ratio (DR), which is a ratio of the earthquake damage repair cost to the total value of a building.

3. Dam's structure and development

Dam's purpose is to hold the pressure from the water for a very long time. Since hydrostatic pressure has a bigger value as the water gets deeper, the dam designer has to calculate the pressure that will be applied to the dam's back surface[32,33]. The dam's structure will look like a right triangle from the side view. The reason behind that is as the depth of the water gets deeper, the hydrostatic pressure will get bigger, and the dam's structure at the bottom will have a longer surface to hold the hydrostatic pressure. The simulation will use Koyna dam as the dam's structure design, which has a water level of 91.72 m. Therefore, the hydrostatic pressure at the bottom of the gravity dam can be obtained from the Eq. 1.

$$P_h = \rho \times g \times h \tag{1}$$

where P_h is hydrostatic pressure, ρ is density of water, g is the gravity of earth, and h is the water level at the gravity dam.

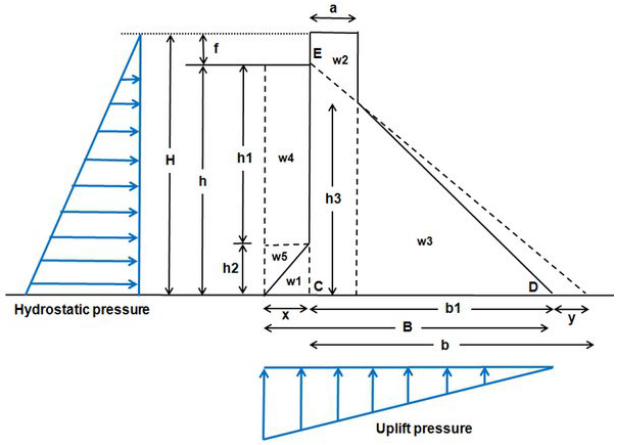

Fig. 1: Working forces on a dam design[32].

where H is the height of dam, h is the height of water surface, b is the base width of the profile from no tension criteria, a is top width provided, f is free board, $h1$ is the depth up to which vertical upstream face is provided, $h2$ is the height of upstream batter from the base, x = a/x1 is the width of upstream batter, $h3$ is the height of downstream sloping face from the base, $y = a/y1$ is the base width reduced in the downstream, $w1$, $w2$, $w3$ is weight of dam, $w4$, $w5$ is weight of water supported by upstream face.

Figure. 1 shows the hydrostatic pressure applied to the dam's structure. As a gravity dam is designed so that its weight and thickness can hold the pressure applied to the structure, the downstream face will usually be a uniform slope, which, if extended, would intersect the vertical upstream face. This is also why the downstream face has to be thicker as it gets to the bottom. The purpose of it is to hold the hydrostatic pressure that is applying bigger forces as it gets to the bottom of the dam's structure. The upstream face will normally be vertical to concentrate most of the dam's weight near the upstream face to overcome tensile stress due to the reservoir water loading. At the same time, thickness is also an important factor in resisting sliding and can dictate the slope on the downstream face.

As hydrostatic pressure is applied on the dam's upstream face, another external force will affect the gravity dam's development. Uplift pressure is an external force applied on the bottom part of the gravity dam. This pressure happens when the water stored on the dam's upstream face enters the pores, fissures, and cracks of the foundation material under pressure, where it also enters the joint between the dam and the foundation itself. This uplift pressure creates a hydraulic gradient between the dam's upstream and downstream face, causing vertical upward pressure that will work against the dam's weight. As the uplift pressure will reduce the effective weight of the gravity dam, engineers have to calculate the effect of the uplift pressure so that the gravity dam still has the stability to hold hydrostatic pressure with its natural weight.

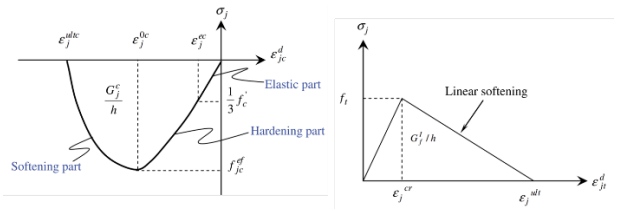

Fig. 2: Working forces on a dam design[34].

The majority of the dam's material is concrete, so it is important to know the nonlinear behavior of concrete under tension and compression load, as shown in Fig. 2. Concrete under compressive load experiences a linear behavior first until the elastic strain ($\varepsilon_{elastic}$), as the load increases, the concrete gets into the hardening part which continues up to the peak strain (ε_{peak}) as the concrete

reaches the maximum strength. After increasing the load, concrete starts to be softened until the ultimate strain ($\varepsilon_{ultimate}$) completely collapses[35]. These parameters are calculated in Eqs. 2-4[36]:

$$\varepsilon_{elastic} = \frac{1}{3}\frac{f_c}{E} \tag{2}$$

$$\varepsilon_{peak} = \frac{4}{3}\frac{\sigma i^{current}}{E} + \varepsilon_{elastic} \quad i = 1.2 \tag{3}$$

$$\varepsilon_{ultimate} = \frac{3}{2}\frac{Gi^{c}}{h\sigma i^{current}} + \varepsilon_{peak} \quad i = 1.2 \tag{4}$$

where f_c is the uniaxial compressive strength of concrete, Gi^c is the current compressive fracture energy of concrete, $\sigma i^{current}$ is the current compressive strength in the direction i, and h is the crack bandwidth, which is calculated with the value $h = \sqrt{2A}$ (A) is the total area of computational control volume). The equivalent uniaxial stress-strain relation in compression is expressed in Eq. 5[35].

$$\sigma^{monotonic} = \begin{cases} E\varepsilon_i \\ \frac{fc}{3}\left[1+4\left(\frac{\varepsilon_i}{\varepsilon_{peak}-\varepsilon_{elastic}}\right)-2\left(\frac{\varepsilon_i-\varepsilon_{elastic}}{\varepsilon_{peak}-\varepsilon_{elastic}}\right)^2\right] \\ \sigma_i^{current}\left[1-\left(\frac{\varepsilon_i-\varepsilon_{peak}}{\varepsilon_{ultimate}-\varepsilon_{peak}}\right)^2\right] \\ 0 \end{cases} \begin{matrix} \varepsilon_{elastic} \le \varepsilon_i \le 0 \\ \varepsilon_{peak} \le \varepsilon_i < \varepsilon_{elastic} \\ \varepsilon_{ultimate} \le \varepsilon_i < \varepsilon_{peak} \\ \varepsilon_i < \varepsilon_{ultimate} \end{matrix} \tag{5}$$

While concrete under pure tension, according to Fig. 2(b), it supposed that the stress-strain relation is entirely linear, so the uniaxial tension strength increases until the critical strain (ε_{cr}) and then starts to decrease until maximum strain (ε_{max}), which is calculated by Eqs. 6 & 7.

$$\varepsilon_{cr} = \frac{fi}{E} \tag{6}$$

$$\varepsilon_m = \frac{2G_f^I}{hf_i} \tag{7}$$

where f_i is the uniaxial tension strength of concrete and G_f^I is the mode 1 fracture energy. The equivalent uniaxial stress-strain relation in tension is calculated by using Eq. 8[37].

$$\sigma_i^{monotonic} = \begin{cases} E\varepsilon_i \\ 1-\left(\frac{\varepsilon_i-\varepsilon_{cr}}{\varepsilon_{max}-\varepsilon_{cr}}\right)^2 \\ 0 \end{cases} \begin{matrix} \varepsilon_{cr} \ge \varepsilon_i \ge 0 \\ \varepsilon_{max} \ge \varepsilon_i > \varepsilon_{cr} \\ \varepsilon_i > \varepsilon_{max} \end{matrix} \tag{8}$$

4. Benchmark particulars

4.1 Profile of the experiment

Finite element analysis is widely utilized in various applications to investigate the behavior of a system or construction[38,39]. The benchmark of this study used ABAQUS software[22] to analyze the seismic response of gravity dam with strain rate effect. Using two types of models, one considering strain rate and the other model without considering strain rate. This study also used a variation on the earthquake's peak to obtain the influence of concrete strain rate on seismic response under different peak accelerations. The results of this study used displacement and acceleration graphics from each model and the earthquake's peak. This graphic was then used to compare to obtain validation for this paper. The benchmark simulation used strain rate consideration to find the strain rate's influence on the gravity dam's seismic response and the strain rate setting in the properties section of ABAQUS software[22]. As the simulation eliminates the influence of the dam foundation, the boundary condition on the stress of the dam body, the foundation extends down 1.5 times the dam height from the bottom of the dam[12].

4.2 Current setting and results

The model that is used in the reference journal simulation is divided into eight nodes hexahedron linear reduction integral element (C3D8R) available in ABAQUS software[22], in which there are 15.200 units of the dam body and 21.660 units of foundation with a total of 39958 nodes with material properties of Koyna Dam is shown in Table 1. The load applied to the model includes static and seismic. The dam's weight and water pressure on the dam's upstream face are static loads, whereas the horizontal and vertical accelerations of earthquakes are defined as the seismic load and applied on the bottom part of the dam. The seismic load refers to a real accident in 1967 where the Koyna dam suffered 6.7 magnitude earthquake, the epicenter distance was 13 km, and the water level in the front of the dam was 91.7 m. So, the measured seismic wave of the Koyna dam under the earthquake disaster was used in the model. The horizontal peak acceleration selected 0.67g, 0.474g, 0.60g, 0.70g, and 0.80g, while the vertical acceleration peak corresponded to 0.15g, 0.24g, 0.312g, 0.39g, 0.46g, and 0.53g.

Figure. 3 and 4 show the displacement and acceleration comparison between the benchmark results and the current results to validate this recent work. Model I (Fig. 3) is the model without considering strain rate. Meanwhile, model II (Fig. 4) considered the concrete strain rate. It can be concluded that the current works successfully presented similar results compared to the provided data by Hai-tao et al.[12]. The time when maximum displacement occurred was found to be similar to Model I; the time range is summarized between 4 to 6 s. The most similar pattern was taken from horizontal and vertical displacements under 0.474g. A similar pattern was also observed in model II, where the peak displacement

occurred in the 3 to 7 s range. Both the horizontal and vertical directions of this model suggested satisfaction, which is the methodology of this work, which can be used further to investigate parameter influences on the structural behaviors under seismic loading.

Table 1. Material properties of Koyna dam, as refereed in Hai-tao et al.[12)]

Geometries	Elastic modulus (GPa)	Poisson's ratio (-)	Density (kg/m^3)	Static compressive strength (MPa)	Static tensile strength (MPa)
Dam Body	31.2	0.2	2642	20.26	1.59
Bedrock	30.0	0.2	2600	-	

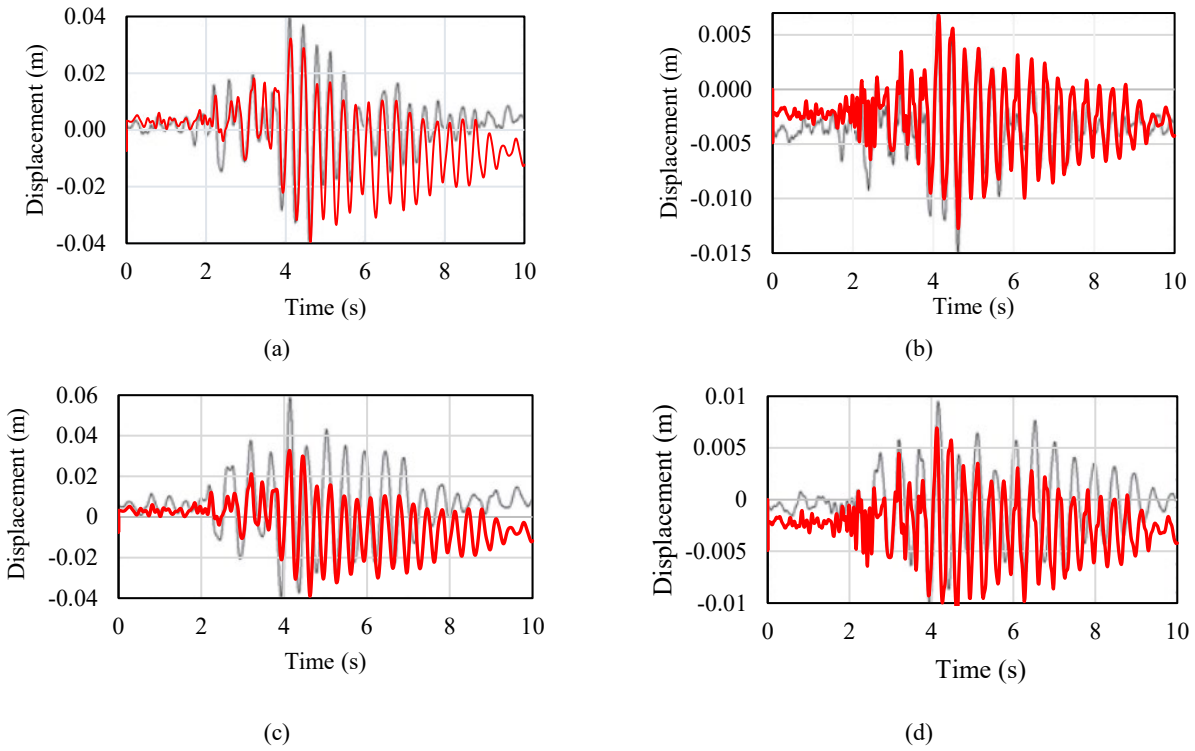

Fig. 3: (a). Horizontal displacement comparison under 0.474g (Model I); (b). Vertical displacement comparison under 0.474g (Model I); (c). Horizontal displacement comparison under 0.8g (Model I); and (d). Vertical displacement comparison under 0.8g (Model I). The grey lines are pioneer works of Hai-tao et al.[12)] and the red lines are provided based on the current study.

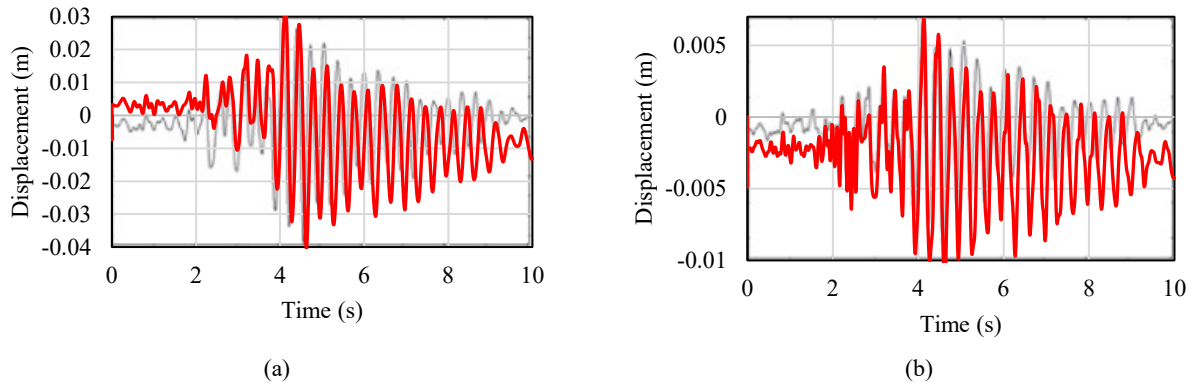

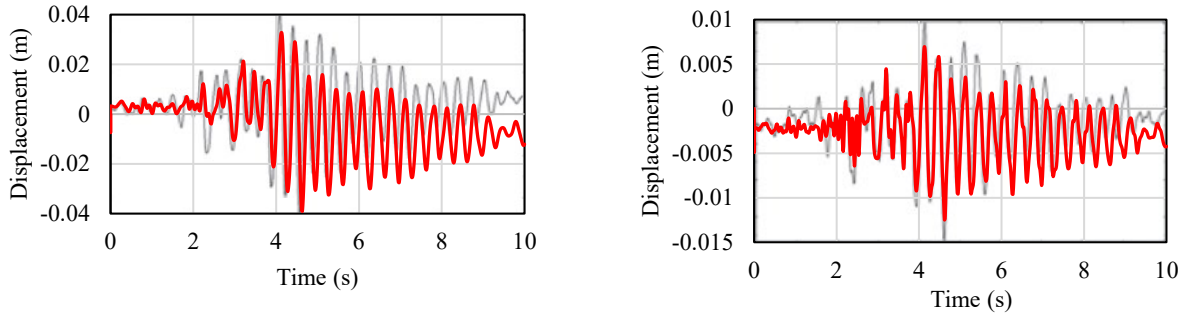

(c) (d)

Fig. 4: (a). Horizontal displacement comparison under 0.474g (Model II); (b). Vertical displacement comparison under 0.474g (Model II); (c). Horizontal displacement comparison under 0.8g (Model II); and (d). Vertical displacement comparison under 0.8g (Model II). The grey lines are pioneer works of Hai-tao et al.[12], and the red lines are provided based on the current study.

5. Method

5.1 Material and geometry

This simulation used concrete as the material of the gravity dam. The purpose of using concrete as the material for gravity dams is because of its density since gravity dams are massive dams composed of a large volume of concrete that holds a large amount of water. Therefore, gravity dams need to bear their own weight. Properties from the concrete have been input for the gravity dam analysis using ABAQUS[22,40-44]. The static calculation parameters utilized in the model are provided in Table 1 , as referred in Hai-tao et al.[12], and the concrete strength of the dam body is measured by uniaxial tension and uniaxial compressive strength at quasi-static strain rate, with the linear elastic model being applied. The properties module gives a plastic-damage model of the concrete solid part and allows you to input strain rate data. When the element is compressed, the yield stress, inelastic strain, and strain rate are entered into the properties module. When the element is tensioned, the yield stress, cracking strain, and strain rate are entered.

The geometry of the dam model uses ABAQUS software, using the model from the Koyna Dam located in Mumbai, India. The dam has a 103 m height and 91.72 m water level as shown in Fig. 5.

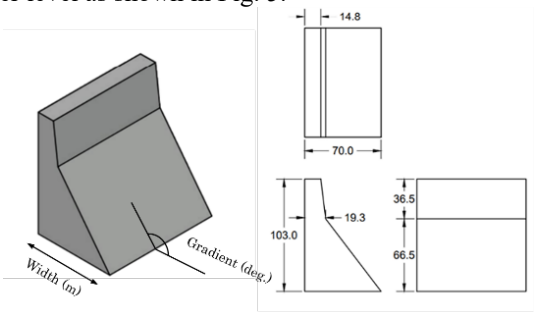

Fig. 5: Gravity dam model

5.2 Boundary condition and FE setting

If a boundary condition is not provided that is comparable to the actual structure, the result may change and yield different forces than those in reality[45-49]. Two main loads are applied to the dam's structure in this case. As the dam uses weight to hold upstream water, gravity plays an important role. Therefore, the first load applied to the dam's structure is gravity load with 9.81 m/s^2 acceleration on the Y axis. The second load is hydrostatic pressure applied at the dam's upstream face. As the dam's water level is 91.72 m, the hydrostatic pressure is 900068 N/m^2 applied at the bottom upstream face of the dam. Two boundary conditions are applied to the dam's structure. The first is earthquake forces, divided into horizontal and vertical acceleration applied at the bottom of the dam. The next boundary condition is displacement/rotation on the X and Y axes applied on the dam's bottom part. Figure. 6 shows the load and boundary conditions of this simulation.

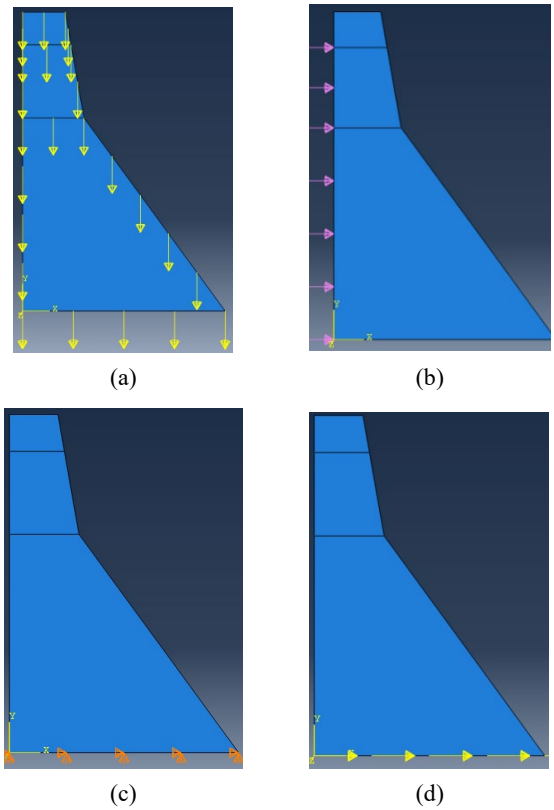

(a) (b)

(c) (d)

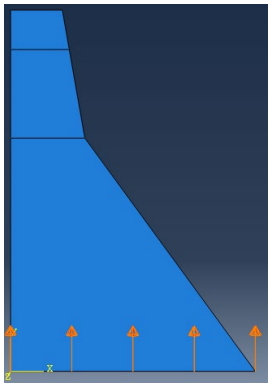

(e)

Fig. 6: Load and boundary condition scheme: (a) gravity load; (b) hydrostatic pressure; (c) displacement/rotation on the x and y axis; (d) horizontal earthquake acceleration; (e) vertical earthquake acceleration.

5.3 Scenario variation

There are two variations related to the dam's structure design: width and gradient variation. A gravity dam's geometry selection, including width and gradient, can significantly influence its strength under seismic loads. The width of the dam base and the slope gradient impact its stability and resistance to overturning against sliding during seismic events. Also, the width and gradient of the dam influence its dynamic response to seismic waves. The geometry of the dam affects its interaction with the reservoir during seismic events. A wider dam may experience different hydrodynamic effects than a narrower one, influencing the distribution of forces and stresses within the structure. In this case, there are four widths: 65 m, 70 m, 75 m, and 80 m. The second variation is the gradient variation. This means the gradient at the dam's neck has several changes, such as 100°, 105°, 110°, and 115°. To have a valid comparison, this paper also has another variation: the earthquake's peak and mesh size.

Selecting an appropriate peak seismic load is crucial to accurately assess the dam's strength and design it to withstand these forces. This variation changes the peak from the original earthquake magnitude and is divided into four variations, i.e., 0.4g, 0.6g, 0.7g, and 0.8g. In addition, choosing an appropriate mesh size ensures that the model accurately represents the complex geometry and behavior of the dam under various loading conditions, leading to more reliable assessment results. In this case, mesh size ranging from 500-1400 mm is evaluated. The overall flowchart of the current investigation is depicted in Fig. 7.

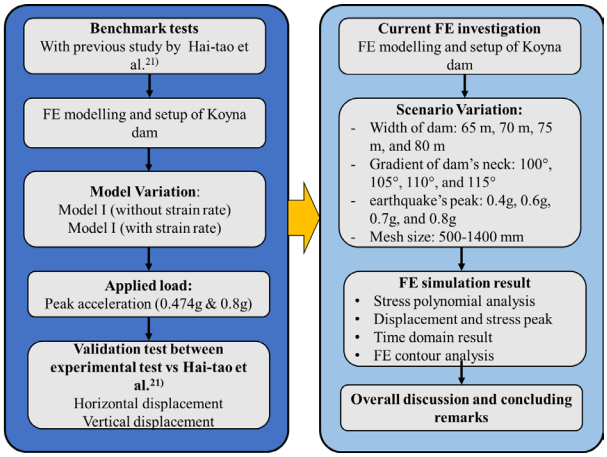

Fig. 7: Overall flowchart of current investigation.

6. Result and discussion

6.1 Stress polynomial analysis

Simulation analysis of the gravity dam has several results that will be analyzed in this work. This section will discuss the polynomial of stress result on the highest stress point on each variation. This analysis aims to find the variation with the lowest stress response value to the earthquake magnitude. The results of the polynomial response to earthquakes are presented in Fig. 8.

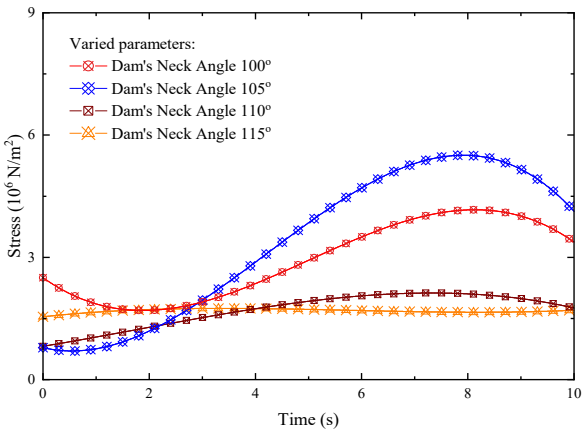

(a)

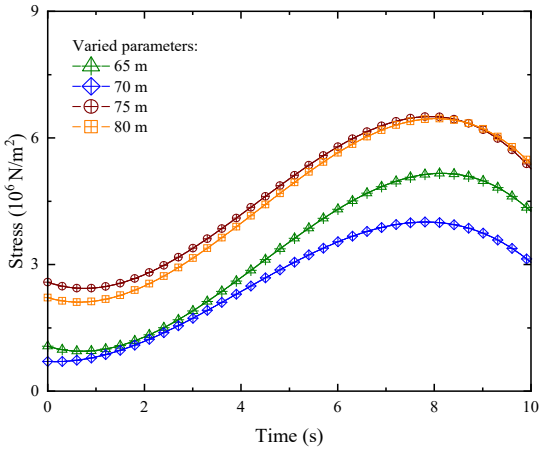

(b)

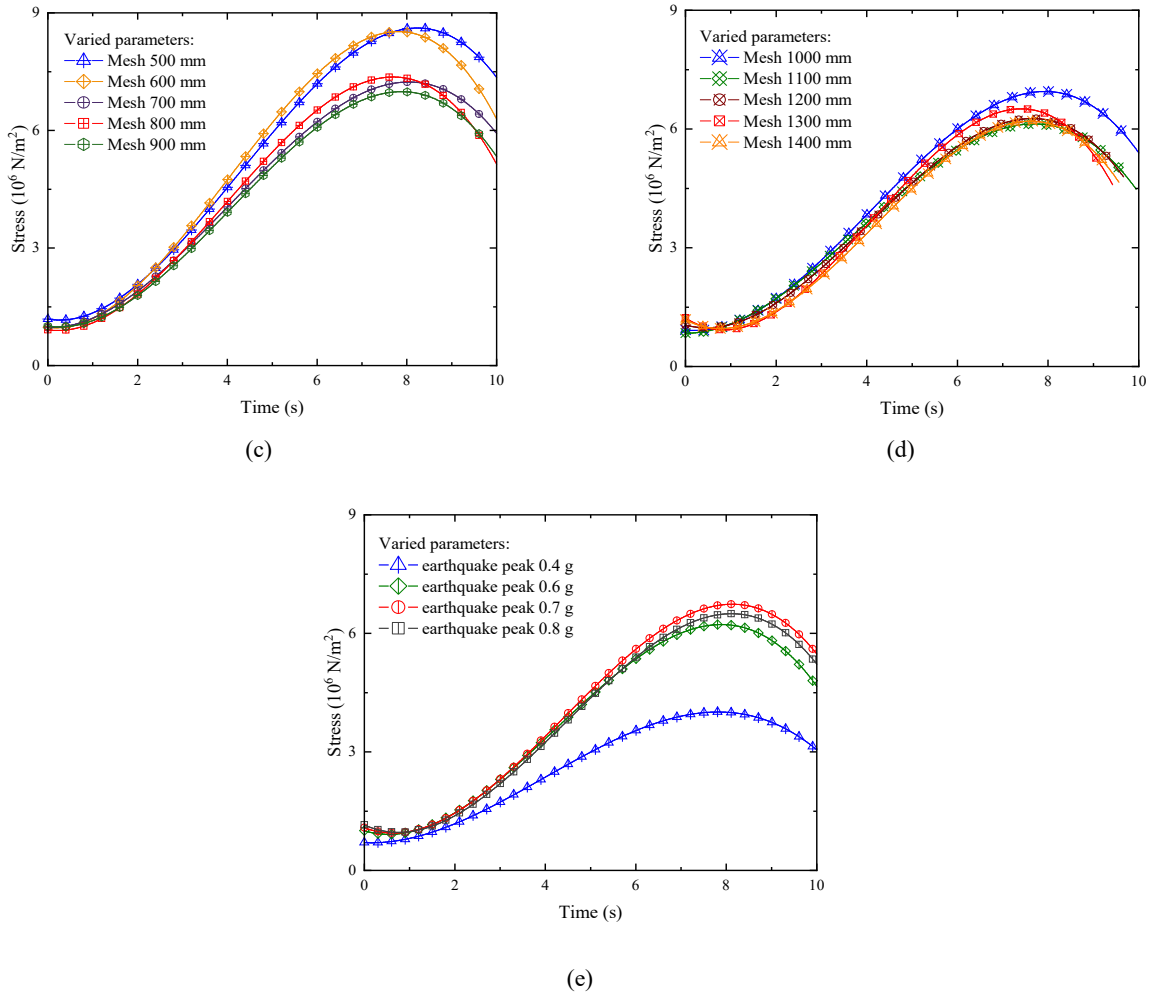

Fig. 8: Polynomial stress over time: (a) gradient variation in °; (b) width variation in m; (c) mesh variation 500-900 mm; (d) mesh variation 1000-1400 mm; (e) earthquake's peak variation.

According to Fig. 8(a), the highest difference of stress value in the results of the polynomial graphic stress of seismic simulation on gradient variation is 4.8 x 10^6 N/m^2, which occurs on 100º gradient variation. Meanwhile, the lowest difference in stress value of the polynomial graphic stress on gradient variation is 0.17 x 10^6 N/m^2, which occurs on 115º gradient variation. Figure 8(b) shows that the stress value peak is 6.5 x 10^6 N/m^2, which occurs on 75 m width variation with a difference between the lowest point and the highest point of 4.07 x 10^6 N/m^2. Meanwhile, the lowest stress peak on width variation is 4 x 10^6 N/m^2, which occurs on 70 m variations with a difference between the lowest and highest points of 3.3 x 10^6 N/m^2.

Figure 8(c) and (d) show that the stress value peak is 8.6 x 10^6 N/m^2, which occurs on 500 mm mesh variation with a difference between the lowest point and the highest point of 7.43 x 10^6 N/m^2. Regarding the lowest peak, stress on mesh variation is 6.19 x 10^6 N/m^2, which occurs on 1000 mm mesh variation with the difference between the lowest point and the highest point 6.48 x 10^6 N/m^2. Figure 8(e) shows that the stress value peak is 6.73 x 10^6 N/m^2, which occurs on a 0.7g earthquake's peak variation with a difference between the lowest point and the highest point of 5.79 x 10^6 N/m^2. On the other hand, the lowest stress peak on an earthquake's peak variation is 4 x 106 N/m^2, which occurs on 0.4g earthquake's peak variation with a difference between the lowest point and the highest point of 3.3 x 10^6 N/m^2.

6.2 Displacement and stress peaks analysis

Figure 9 compares the displacement and stress peaks of each variation. This section will discuss how much the variation affects displacement and stress related to the seismic response. Figure 9(a) compares displacement and stress in gradient variation analyzed in width 80 m, mesh size 700 mm, and earthquake's peak 0.4g. The result shows that the highest displacement point is 0.361 m, which occurs in a 105° gradient variation, and the lowest is 0.352 m, which occurs in a 100° gradient variation. Meanwhile, the highest stress point is 11.19 x 10^{10} N/m^2, which occurs in 100º gradient variation, and the lowest point is 3.07 x 10^6 N/m^2, which occurs in 115° gradient variation. It also shows from the stress trend line that the bigger the gradient, the bigger the stress value.

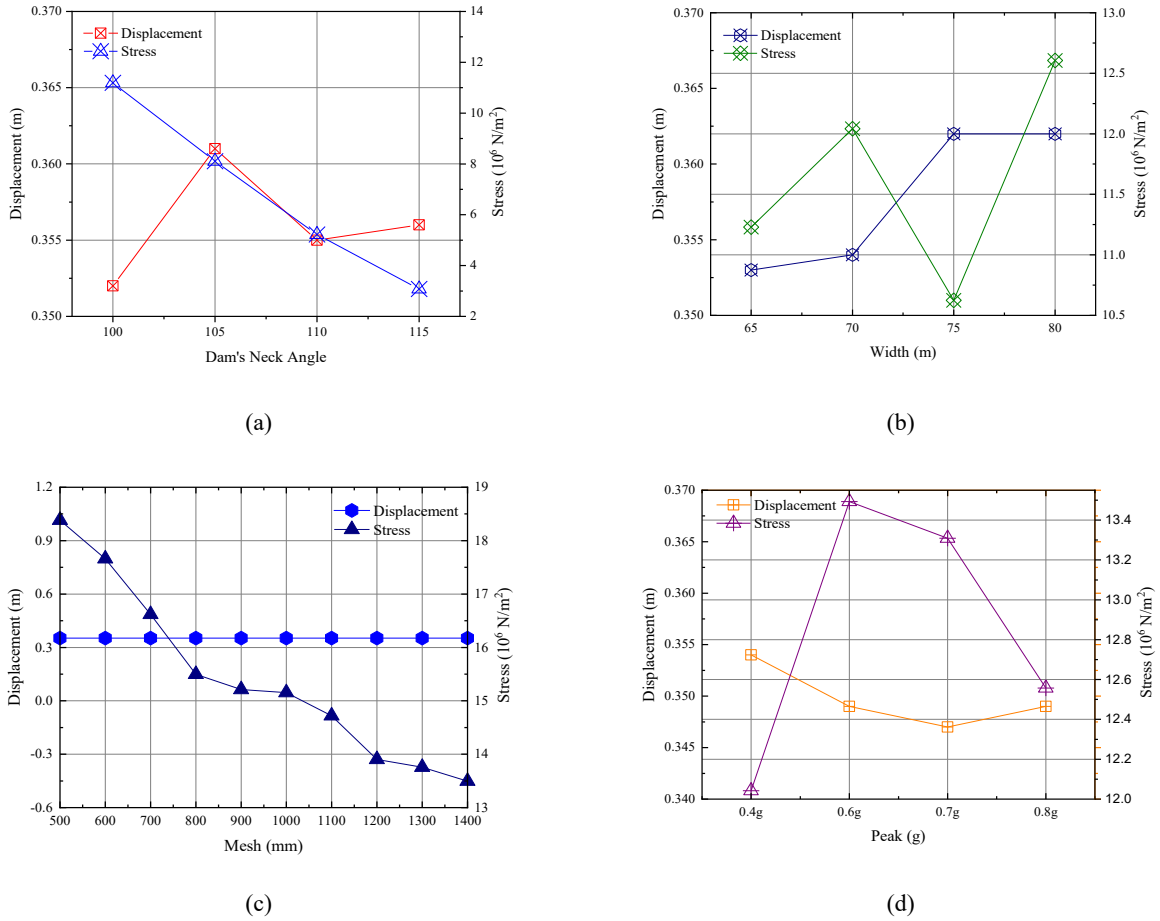

Fig. 9: Displacement and stress peak: (a) gradient variation in °; (b) width variation in m; (c) mesh variation; and (d) earthquake's peak variation.

Figure 9(b) compares displacement and stress in width variation analyzed in gradient 100°, mesh size 700 mm, and earthquake's peak 0.4g. The highest displacement point is 0.362 m, which occurs in 75 m and 80 m width variations, and the lowest is 0.353 m, which occurs in 65 m width variations. Meanwhile, the highest stress point is 12.6 x 10^6 N/m^{2,} which occurs in 80 m width variation, and the lowest stress point is 10.62 x 10^6 N/m^{2,} which occurs in 75 m width variation. Figure 9(c) compares displacement and stress in mesh variation analyzed in gradient 100°, width 80 m, and earthquake's peak 0.4g. The highest and lowest displacement points in mesh variation are 0.352 m since all the variations have the same value. Meanwhile, the highest stress point is 18.38 x 10^6 N/m^{2,} which occurs in 500 mm mesh variation, and the lowest is 13.48 x 10^6 N/m^{2,} which occurs in 1400 mm mesh variation. Figure 9(d) compares displacement and stress in earthquake peak variation analyzed in gradient 100°, width 80 m, and mesh size 700 mm. The highest displacement is 0.354 m, which occurs in the 0.4g earthquake's peak variation, and the lowest is 0.347 m, which occurs in the 0.7g earthquake's peak variation. As shown in the result, from 0.4g until 0.7g variation, the trend line goes down, and then when it hits 0.8g variation, it goes up 0.002 m from the previous position. Since the difference between the highest and lowest point of displacement is too small (0.007 m), the displacement result of the earthquake's peak variation is stable. Meanwhile, the highest point of the stress result of the earthquake's peak variation is 13.49 x 10^6 N/m^{2,} occurs in 0.6g, and the lowest point is 12.04 x 10^6 N/m^{2,} with the difference between the highest and the lowest point being 1.45 x 10^6 N/m^2.

6.3 Time domain response

This section shows time response seismic simulation result of each variation. The results are obtained from the highest point of stress on each variation. This graphic was used previously for the polynomial graphics, which are shown in Fig. 8. Fig. 10(a) shows the stress result on gradient variation evaluated at width 80 m, mesh size 700 mm, and earthquake's peak 0.4g. It shows that gradient 115° and 110° have the lowest value of stress, while 100° and 105° have a bigger stress value. Figure 10(b) shows the results on width variation evaluated at gradient 100°, mesh size 700 mm, and earthquake's peak 0.4g. As the width gets longer, the stress value also gets bigger. Figure 10(c) shows the results of mesh variation analyzed in gradient 100°, width 80 m, and earthquake's peak 0.4g.

The smaller the mesh size, the bigger the stress value is. Fig. 10(d) shows the earthquake's peak variation results analyzed in gradient 100°, width 80 m, and mesh size 700 mm. The stress value on the dam's body increases as the peak increases.

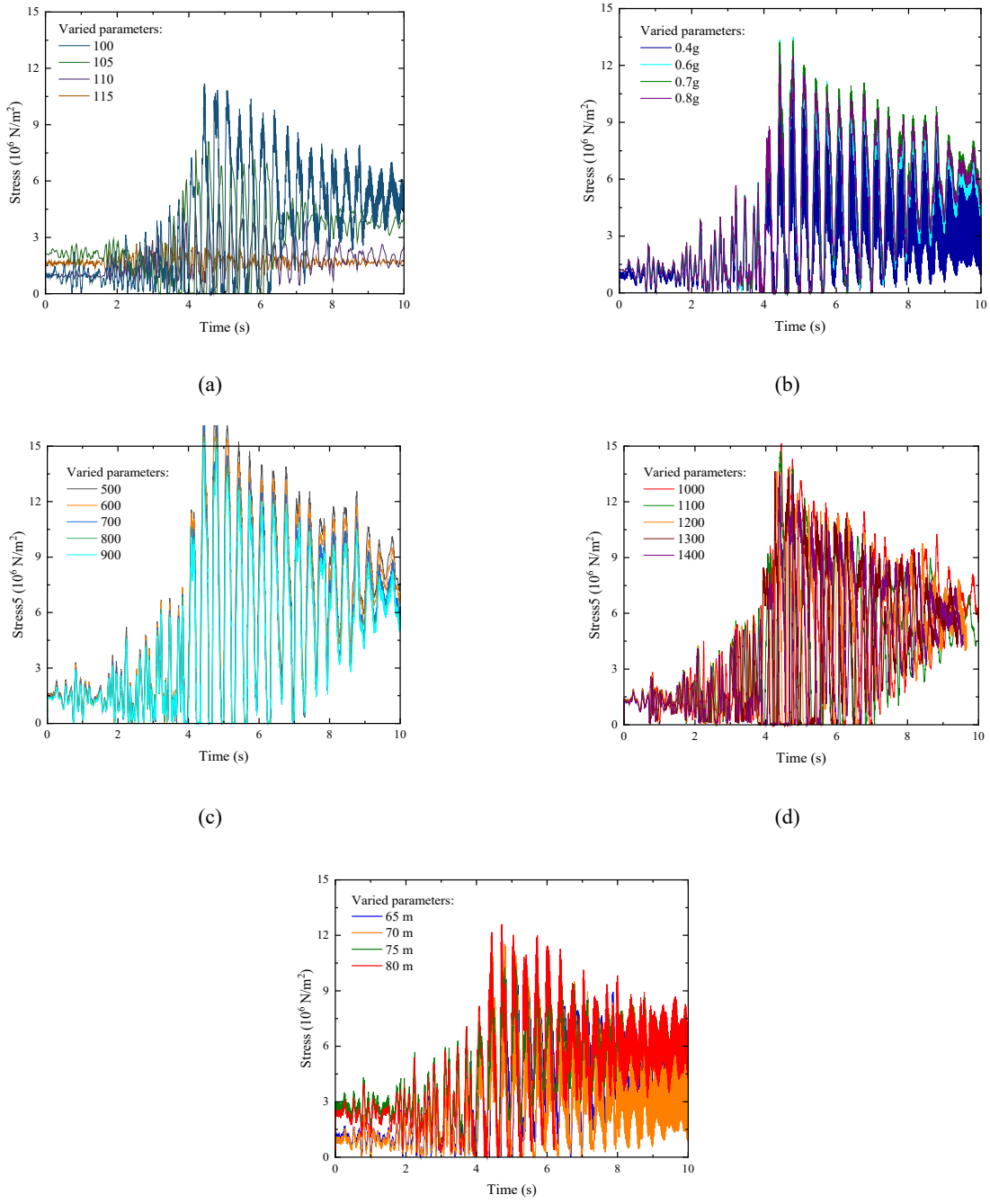

Fig. 10: Displacement and stress peak: (a) gradient variation in °; (b) width variation in m; (c) mesh variation-1; (d) mesh variation-2 and (e) earthquake's peak variation.

6.4 Stress and displacement contour analysis

This section will compare and analyze the contour result from the seismic simulation of a gravity dam. Since this section will discuss three indicators (displacement, stress, and tensile damage), there are 66 contours to compare for all the variations. Therefore, to simplify the analyzing process, the writer used two contours for each variation on each indicator. The contour used in this section will be the smallest and largest versions in each variation.

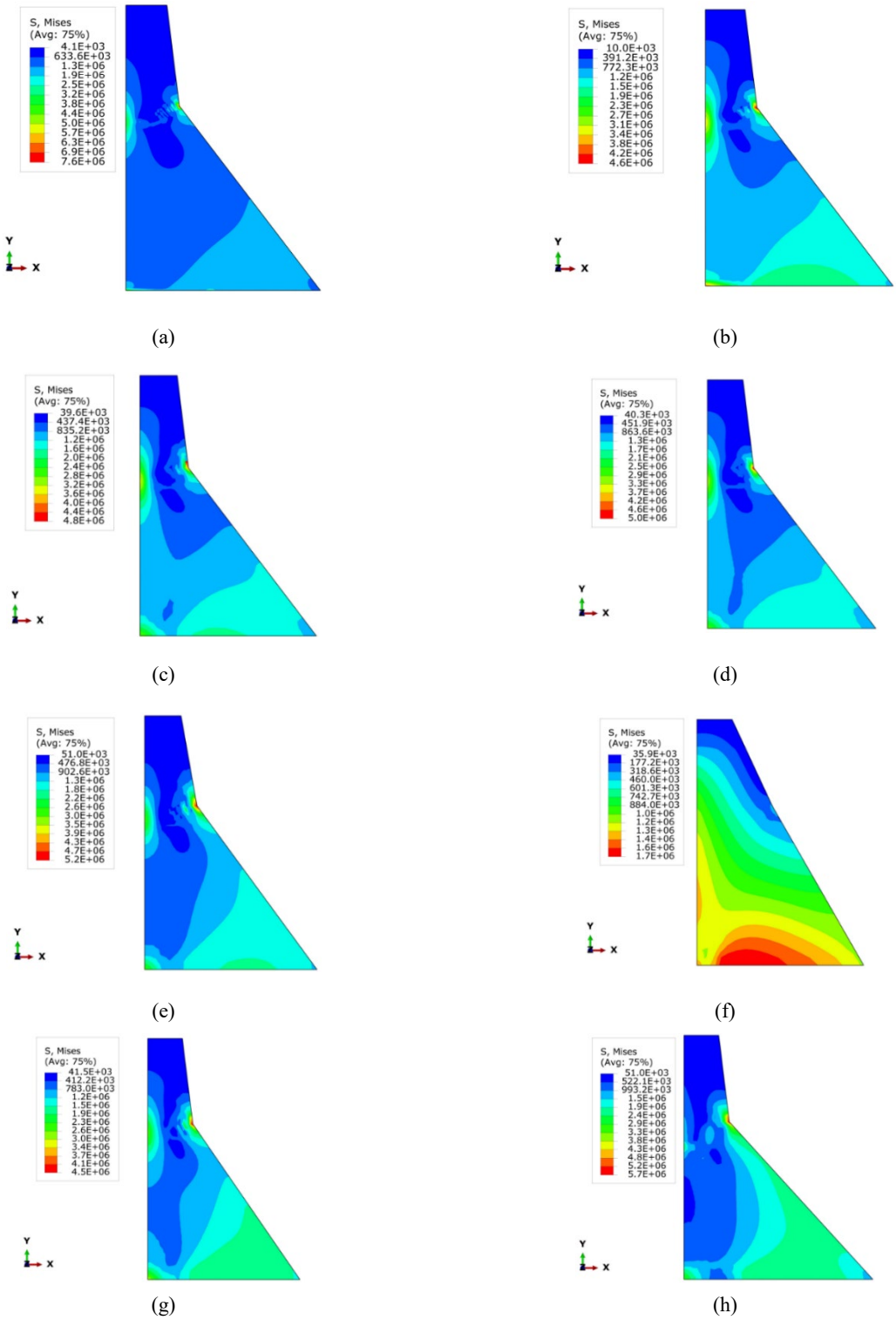

Fig. 11: Stress contour result: (a) mesh 500 mm; (b) mesh 1400 mm; (c) peak 0.4g; (d) peak 0.8g; (e) gradient 100°; (f) gradient 115°; (g) width 65 m; and (h) width 80 m.

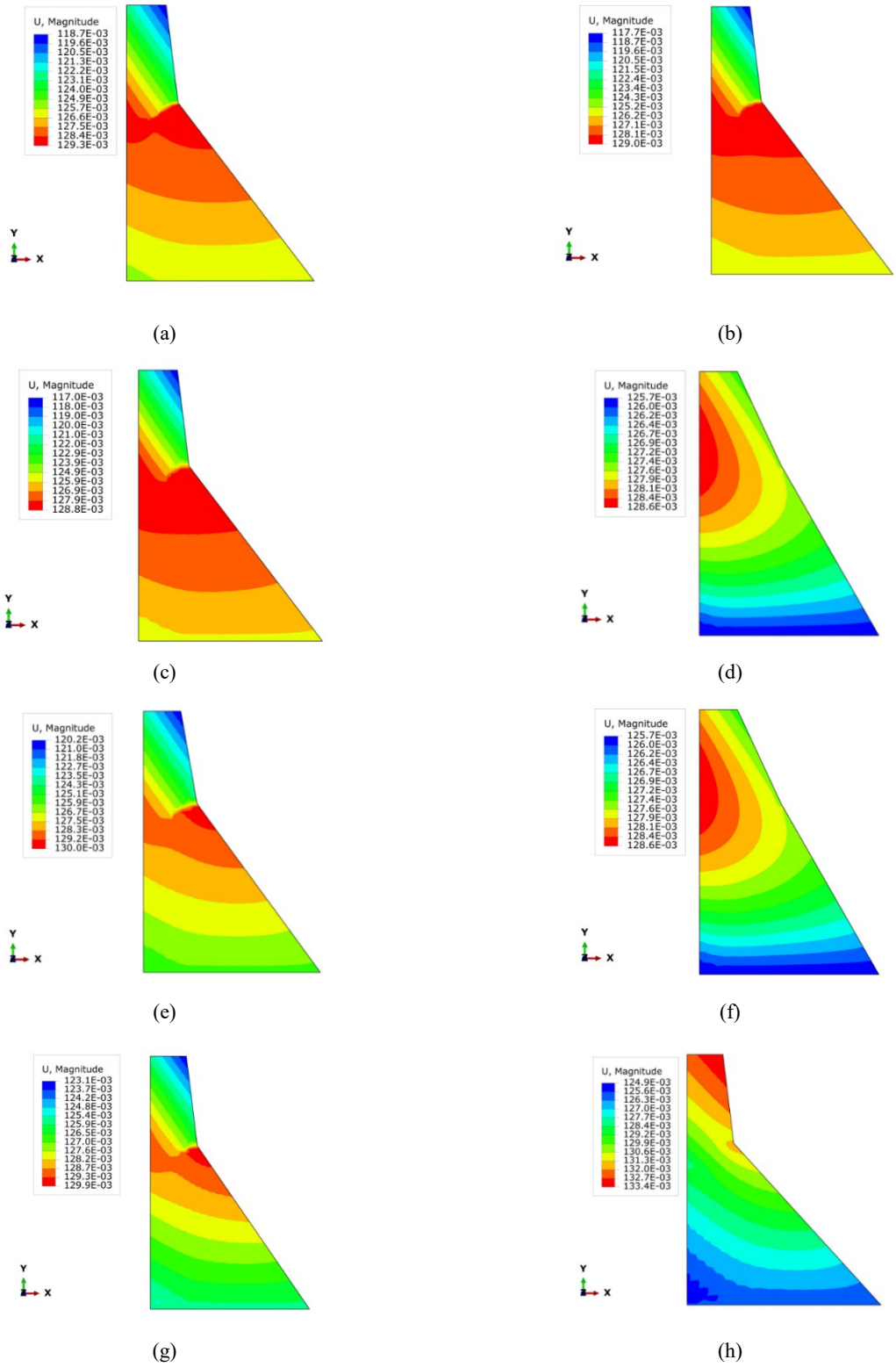

Fig. 12: Displacement contour result: (a) mesh 500 mm; (b) mesh 1400 mm; (c) peak 0.4g; (d) peak 0.8g; (e) gradient 100°; (f) gradient 115°; (g) width 65 m; and (h) width 80 m.

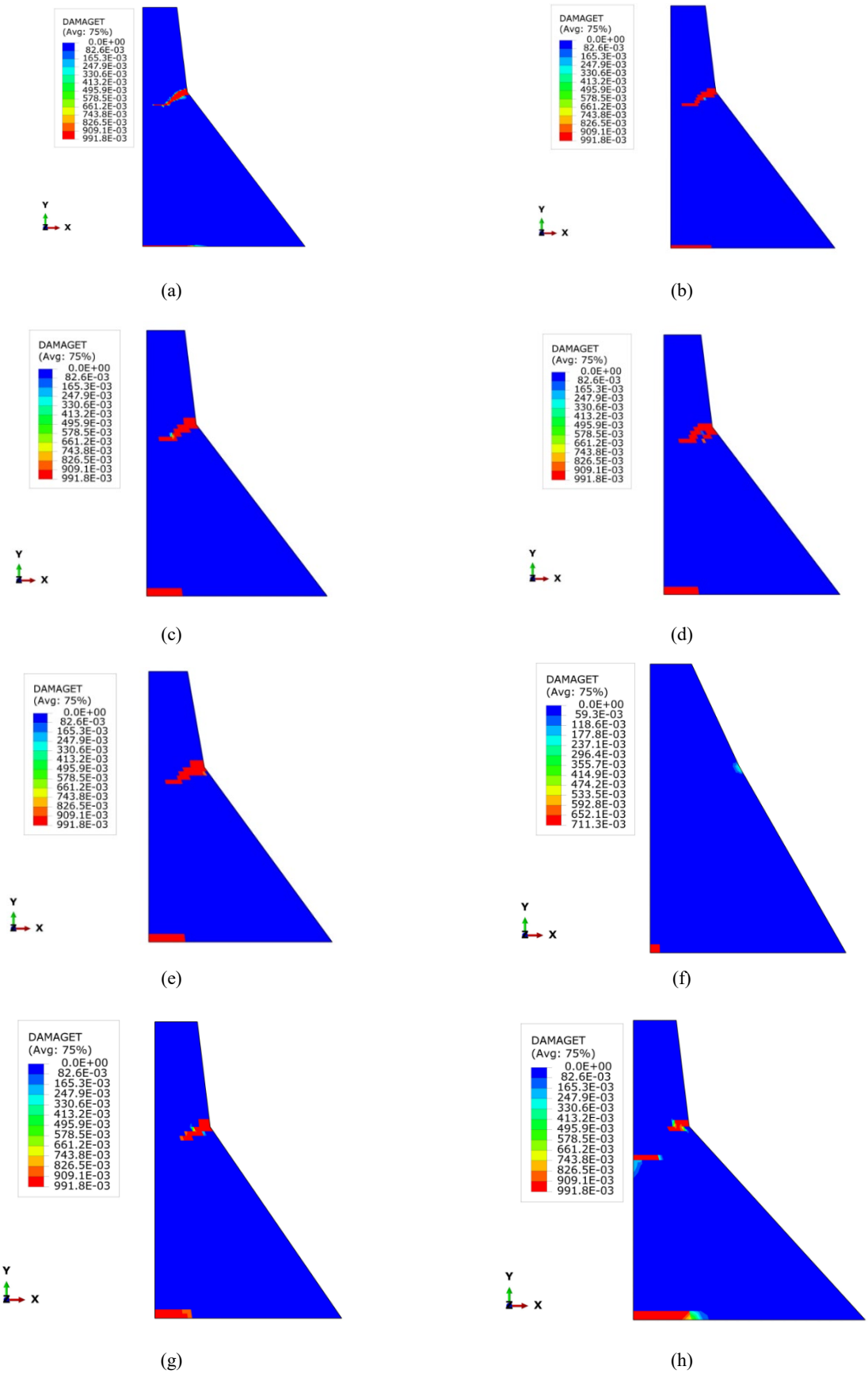

Fig. 13: Tensile damage contour result: (a) mesh 500 mm; (b) mesh 1400 mm; (c) peak 0.4g; (d) peak 0.8g; (e) gradient 100°; (f) gradient 115°; (g) width 65 m; and (h) width 80 m.

The first contour that will be compared is the stress contour result. As we can see in Figs. 11(a) and (b), the stress contour result of the mesh variation is that as the mesh size gets bigger, the stress distribution on the back and bottom sides of the gravity dam gets longer. The highest stress point for the 500 mm mesh variation is 7.6 x 10^6 N/m^2, while the highest stress point for the 1400 mm mesh variation is 4.6 x 10^6 N/m^2. Figure. 11(c) and (d) show the stress contour result of an earthquake's peak variation, and this result will show how the gravity dam reacts to the difference in an earthquake's peak. The highest stress point on 0.4g variation is 4.8 x 10^6 N/m^2, while the highest stress point on 0.8g variation is 5 x 10^6 N/m^2. It showed that as the earthquake's peak grew, the gravity dam's stress reaction also increased. Figure 11(e) and (f) show the stress contour of gradient variation. As shown in Fig. 11 above, this variation has several significant differences. As we observe the 115° gradient variation, the stress distribution is very different from other variations where the highest stress point is located at the bottom of the dam. This shows that as the gradient gets bigger, the stress distribution will lead to the bottom part of the dam. Even though this tells us that there is a smaller risk the dam will break in the center, the bottom part of the dam is where the biggest hydrostatic pressure happened on the dam. Figure. 11(g) and (h) show the stress contour of width variation. As we can see from Fig. 11 above, as the width gets longer, the stress value on the bottom part of the dam gets smaller. This means that the width of the dam will resist the hydrostatic pressure applied on the back side of the dam.

Figure 12 discusses the comparison of a displacement's contour. From Figs. 12(a) and (b), there is no significant difference between the displacement contour results on mesh variation as they have similar values on the highest displacement point. Figure 12(c) and (d) show the displacement contour result of the earthquake's peak variation. The 0.8g earthquake's peak variation has a displacement distribution majority on the dam's crest or the top part of the dam, while the 0.4g earthquake's peak variation has a displacement distribution majority on the dam's body. Figure 12(e) and (f) show the displacement contour result of gradient variation. While the 100° gradient variation has a similar contour to other variations, the 115° gradient variation has a significant difference where most of the displacement happened on the back side of the dam. Figure 12(g) and (h) show the displacement contour result of width variation. As the 65 m width variation has a similar contour to other variations, the 80 m width variation has a smaller displacement value on the bottom part of the dam but a higher displacement value on the crest or the top part.

Figure 13 discusses the comparison of a tensile damage contour, Figs. 13(a) and (b) show the tensile damage contour of mesh variation. As shown in Fig. 13 above, the 500 mm and the 1400 mm mesh variations have a similar tensile damage value. Figure. 13(c) and (d) show the tensile damage of the earthquake's peak variation. While they have a similar tensile damage value, the 0.8g earthquake's peak variation has a little branch of tensile damage on the dam's neck, while the 0.4g earthquake's peak variation doesn't have a similar contour to other variations. Figure 13(e) and (f) show the tensile damage of gradient variation. While the 100° variation has a similar contour, the 115° has a significant difference, as we can see on the dam's neck of 115° variation, they have a very small value of tensile damage compared to other variations, this means the bigger gradient on the dam's neck will reduce the tensile damage. Figure 13(g) and (h) show the tensile damage of width variation; the 65 m variation has a similar contour, and the 80 m variation has several differences, while other varieties have a tensile damage majority on the dam's neck on the front side, the 80 m variation has two part of tensile damage that happens on the front and the back side on the dam's neck.

6.5 Overall Discussion

Results on the polynomial section from Fig. 7(a) show that the dam's gradient will affect the result from seismic simulation, as the two highest gradient variations have a similar polynomial stress value that also has the lowest difference stress value. This shows that 115° and 110° gradient variations have good resistance and stability to earthquake forces compared to 105° and 100° gradient variations. As the polynomial shows the advantage of a bigger gradient on the gravity dam, Fig. 9(f) shows that the stress distribution on the bigger gradient variation mostly occurred on the dam's bottom part. This shows the disadvantage of a bigger gradient on the gravity dam, where the bottom part will likely break first. This is not good, considering if the bottom part breaks first, then all the water and the gravity dam will also break and endanger the downstream part of the dam.

As a gravity dam is designed to hold the water on the vertical upstream face, engineers usually design the downstream face as a uniform slope, which helps to hold the hydrostatic pressure as the highest hydrostatic pressure is located on the bottom of the dam. This leads to the effects of the dam's width to hold the hydrostatic pressure. Figure 12(g) and (h) show stress distribution contour on width variation. There is no other significant difference besides the highest stress value on each contour. At the same time, Fig. 13(g) and (h) show the majority of displacement during the earthquake happened on the dam's crest. Figure 13(g) and (h) also show the disadvantage of having a longer width. While the tensile damages on the dam's neck are thinner, apparently, on the upstream face appeared tensile damages that most other variations don't have. This proves that width variation affects the dam's behavior on seismic simulation, as it can hold the hydrostatic pressure better as the width gets longer. It also has a disadvantage that occurred on the upstream face.

7. Conclusions

This study aims to investigate various design factors crucial for enhancing the earthquake resistance and structural integrity of gravity dams. Findings reveal that both gradient variation at the dam's neck and changes in dam width significantly influence the dam's response to seismic events. While adjusting the gradient can mitigate stress concentration at the dam's neck, an excessive gradient may exacerbate stress distribution at the dam's base, potentially leading to catastrophic failure during earthquakes, which often initiate from the bottom. Similarly, altering the width of the dam offers a strategy to alleviate stress on its lower portion. However, increasing width may redirect tensile damage towards the upstream face, increasing the risk of dam failure during seismic activity.

Although perfection is unattainable, this study maximizes insights to inform further research endeavors. Moreover, it serves as a foundational reference for evaluating the seismic performance of gravity dams with overflow sections, offering valuable considerations for future investigations. Building upon existing research in gravity dam seismic simulations, this study provides a crucial link to future experiments, facilitating a more comprehensive understanding of dam behavior under seismic loading.

Acknowledgment

This work was supported by the RKAT PTNBH Universitas Sebelas Maret – Year 2024, under the Research Scheme of "Program Kemitraan Masyarakat" (PKM-UNS), with Research Grant/Contract No. 195.1/UN27.22/PT.01.03/2024. The authors gratefully acknowledge the support.

References

1) A. Narwal, S. Setia, and S N Sachdeva, "Seismic performance and suitability of elastomeric and pot PTFE bearings for girder bridges," *Evergreen*, **10** (*2*) 752–764 (2023), doi:10.5109/6792825.
2) K. Zhang, F. Lu, Y. Peng, and X. Li, "Study on dynamic response of gravity dam under air blast load based on similarity law," *Eng. Fail. Anal.*, **138** 106225 (2022). doi: 10.1016/j.engfailanal.2022.106225.
3) X. Ren, Q. Wang, Y. Chen, J. Wang, and L. Lyu, "Effects of bedrocks on the dynamic response of concrete gravity dams subjected to underwater explosions," *Eng. Fail. Anal.*, **139** 106410 (2022). doi:10.1016/j.engfailanal.2022.106410.
4) H. Mostafaei, M. Sohrabi Gilani, and M. Ghaemian, "Stability analysis of arch dam abutments due to seismic loading," *Sci. Iran.*, **24** (*2*) 467–475 (2017), doi: 10.24200/sci.2017.2410.
5) H. Mostafaei, D. Mostofinejad, M. Ghamami, and C. Wu, "A new approach of ensemble learning in fully automated identification of structural modal parameters of concrete gravity dams: A case study of the Koyna dam," *Struct.*, **50** 255–271 (2023), doi: 10.1016/j.istruc.2023.02.034.
6) C. Lin, T. Li, X. Liu, L. Zhao, S. Chen, and H. Qi, "A deformation separation method for gravity dam body and foundation based on the observed displacements," *Struct. Control Heal. Monit.*, **26** (*2*), e2304 (2019), doi: 10.1002/stc.2304.
7) W. Ge, Y. Qin, Z. Li, H. Zhang, W. Gao, X. Guo, Z. Song, W. Li, and P.V. Gelder, "An innovative methodology for establishing societal life risk criteria for dams: A case study to reservoir dam failure events in China," *Int. J. Disaster Risk Reduct.*, **49** 101663 (2020), doi: 10.1016/j.ijdrr.2020.101663.
8) L. M. Zhang, Y. Xu, and J. S. Jia, "Analysis of earth dam failures: A database approach," *Georisk Assess. Manag. Risk Eng. Syst. Geohazards*, **3** (*3*) 184–189 (2009), doi: 10.1080/17499510902831759.
9) A. K. Chopra, and P. Chakrabarti, "The earthquake experience at koyna dam and stresses in concrete gravity dams," *Earthq. Eng. Struct. Dyn.*, **1** (*2*) 151–164 (1972), doi: 10.1002/eqe.4290010204.
10) O. Omidi, and V. Lotfi, "Seismic plastic–damage analysis of mass concrete blocks in arch dams including contraction and peripheral joints," *Soil Dyn. Earthq. Eng.*, **95** 118–137 (2017), doi: 10.1016/j.soildyn.2017.01.026.
11) N. Oudni, and Y. Bouafia, "Response of concrete gravity dam by damage model under seismic excitation," *Eng. Fail. Anal.*, **58** 417–428 (2015), doi: 10.1016/j.engfailanal.2015.08.020.
12) W. Hai-tao, S. Jiayu, W. Feng, A. Zhiqiang, and L. Tianyun, "Experimental study on elastic-plastic seismic response analysis of concrete gravity dam with strain rate effect," *Soil Dyn. Earthq. Eng.*, **116** 563–569 (2019), doi:10.1016/j.soildyn.2018.09.020.
13) M. Smith, "ABAQUS/Standard User's Manual, Version 6.12," Dassault Systèmes Simulia Corp, Providence, 2012.
14) M. Alembagheri, "Earthquake damage estimation of concrete gravity dams using linear analysis and empirical failure criteria," *Soil Dyn. Earthq. Eng.*, **90** 327–339 (2016), doi:10.1016/j.soildyn.2016.09.005.
15) Ö. Aydan, N.Z. Nasiry, Y. Ohta, and R. Ulusay, "Effects of earthquake faulting on civil engineering structures," *J. Earthq. Tsunami*, **12** (*4*) 1841007 (2018), doi:10.1142/S1793431118410075.
16) Y. Reuland, P. Lestuzzi, and I.F.C. Smith, "An engineering approach to model-class selection for measurement-supported post-earthquake assessment," *Eng. Struct.*, **197** 109408 (2019), doi:10.1016/j.engstruct.2019.109408.
17) Y. Bozorgnia, and V. V Bertero, "Earthquake Engineering: From Engineering Seismology to Performance-Based Engineering," CRC press, Boca

Raton, 2004.
18) K.R.Y. Simha, "Seismic conceptual design of buildings," *Resonance*, **12** (*8*) 82–84 (2007), doi:10.1007/s12045-007-0085-3.
19) F. Omori, "Seismic experiments on the fracturing and overturning of columns," available in: https://repository.dl.itc.u-tokyo.ac.jp/record/38660/files/KJ00004857162.pdf (1990).
20) L. Lu, J. Jia, and Z. Tang, "Structural Mechanics," CRC press, Boca Raton, Florida, 2022.
21) M. Ghaemian and A. Ghobarah, "Nonlinear seismic response of concrete gravity dams with dam–reservoir interaction," *Eng. Struct.*, **21** (*4*) 306–315 (1999), doi: 10.1016/S0141-0296(97)00208-3.
22) G. Sevieri, M. Andreini, A. De Falco, and H. G. Matthies, "Concrete gravity dams model parameters updating using static measurements," *Eng. Struct.*, **196** 109231 (2019), doi: 10.1016/j.engstruct.2019.05.072.
23) A. Kita, A. Lupattelli, I. Venanzi, D. Salciarini, and F. Ubertini, "The role of seismic hazard modeling on the simplified structural assessment of an existing concrete gravity dam," *Struct.*, **34** 4560–4573 (2021), doi: 10.1016/j.istruc.2021.10.037.
24) R.A. Mir, and C.A. Taylor, "An experimental investigation into earthquake-induced failure of medium to low height concrete gravity dams," *Earthq. Eng. Struct. Dyn.*, **24** (*3*) 373–393 (1995), doi: 10.1002/eqe.4290240306.
25) E. Zhao, and C. Wu, "Long-term safety assessment of large-scale arch dam based on non-probabilistic reliability analysis," *Struct.*, **32** 298–312 (2021), doi: 10.1016/j.istruc.2021.03.012.
26) R. Tinawi, P. Léger, M. Leclerc, and G. Cipolla, "Seismic Safety of Gravity Dams: From Shake Table Experiments to Numerical Analyses," *J. Struct. Eng.*, **126** (4) 518–529 (2000), doi: 10.1061/(ASCE)0733-9445(2000)126:4(518).
27) X. Wang, B. Xue, B. Xu, and R. Pang, "Role of strong motion duration on seismic responses of high concrete faced rockfill dams," *Struct.*, **32** 1092–1102 (2021), doi: 10.1016/j.istruc.2021.03.092.
28) Y. Calayir and M. Karaton, "A continuum damage concrete model for earthquake analysis of concrete gravity dam–reservoir systems," *Soil Dyn. Earthq. Eng.*, **25** (*11*) 857–869 (2005), doi: 10.1016/j.soildyn.2005.05.003.
29) O. Omidi, S. Valliappan, and V. Lotfi, "Seismic cracking of concrete gravity dams by plastic–damage model using different damping mechanisms," *Finite Elem. Anal. Des.*, **63** 80–97 (2013), doi: 10.1016/j.finel.2012.08.008.
30) M.. Lindeburg, and M. Baradar, "Seismic Design of Building Structures: A Professional's Introduction to Earthquake Forces and Design Details," Professional Publications Inc, Belmont, 2011.
31) M. Haseeb, A. Bibi, J.Z. Khan, I. Ahmad, and R. Malik, "Construction of earthquake resistant buildings and infrastructure implementing seismic design and building code in northern pakistan 2005 earthquake affected area," *Int. J. Bus. Soc. Sci.*, **2** (*4*) 168–177 (2011).
32) C. Denver, "Design of gravity dams," A Water Resources Technical Publication, Denver, 1976.
33) United States Department of the Interior, "Design of Small Dams," Bureau of Reclamation, Washington, DC, 1987.
34) W. He, Y.-F. Wu, K.M. Liew, and Z. Wu, "A 2d total strain based constitutive model for predicting the behaviors of concrete structures," *Int. J. Eng. Sci.*, **44** (*18–19*) 1280–1303 (2006), doi:10.1016/j.ijengsci.2006.07.007.
35) S.-R. Sabbagh-Yazdi, A. Farhoud, A. Mohammadi, and E. Yazdinasabkarani, "Earthquake damage estimation of the koyna concrete gravity dam using explicit gfvm model considering fluid–structure interaction," *Math. Comput. Simul.*, **195** 151–170 (2022), doi:10.1016/j.matcom.2022.01.002.
36) J.G.M. van Mier, S.P. Shah, M. Arnaud, J.P. Balayssac, A. Bascoul, S. Choi, D. Dasenbrock, G. Ferrara, C. French, M.E. Gobbi, B.L. Karihaloo, G. König, M.D. Kotsovos, J. Labuz, D. Lange-Kornbak, G. Markeset, M.N. Pavlovic, G. Simsch, K.-C. Thienel, A. Turatsinze, M. Ulmer, H.J.G.M. van Geel, M.R.A. van Vliet, and D. Zissopoulos, "Strain-softening of concrete in uniaxial compression," *Mater. Struct.*, **30** (*4*) 195–209 (1997), doi:10.1007/BF02486177.
37) U.A. Ebead, "Tension-stiffening model for frp-strengthened concrete two-way slabs," *Mater. Struct.*, **38** (*276*) 193–200 (2005). doi:10.1617/14089.
38) Muhamad Arjuna Putra Perdana, Sudirja, A. Hapid, A. Muharam, S. Kaleg, Amin, R. Ristiana, and Alexander Christantho Budiman, "Crashworthiness enhancement: the optimization of vehicle crash box performance by utilizing bionic-albuca spiralis thin-walled structure," *Evergreen*, **10** (*3*) 1961–1967 (2023). doi:10.5109/7151754.
39) Lalit N. Patil, Atul A. Patil, Kishor B. Waghulde, Sarika A. Patil, Yashraj M. Patil, Subhash L. Gadhave, Vijaykumar K. Javanjal, and Swapnil S. Jadhav, "Finite element analysis for improved all-terrain vehicle component design," *Evergreen*, **10** (*3*) 1508–1521 (2023). doi:10.5109/7151699.
40) A. Nurcholis, A.R. Prabowo, N. Muhayat, I. Yaningsih, D.D.D.P. Tjahjana, M. Jurkovič, J.M. Sohn, M.I. Hanif, and R. Ridwan, "Performances of the sandwich panel structures under fire accident due to hydrogen leaks: Consideration of structural design and environment factor using FE analysis," *Curve. Layer. Struct.*, **11** (*1*) 20240005 (2024), doi: 10.1515/cls-2024-0005.
41) Q.T. Do, T. Muttaqie, P.T., Nhut, M.T. Vu, N.D. Khoa, and A.R. Prabowo, "Residual ultimate strength

assessment of submarine pressure hull under dynamic ship collision," *Ocean Eng.*, **266** 112951 (2022), doi: 10.1016/j.oceaneng.2022.112951.

42) C.Y.G. Satriawan, A.R. Prabowo, T. Muttaqie, R. Ridwan, N. Muhayat, H. Carvalho, and F. Imaduddin, "Assessment of the beam configuration effects on designed beam-column connection structures using FE methodology based on experimental benchmarking," *J. Mech. Behav. Mater.*, **32** (*1*) 20220284 (2023), doi: 10.1515/jmbm-2022-0284.
43) Q.T. Do, T. Ghanbari-Ghazijahani, and A.R. Prabowo, "Developing empirical formulations to predict residual strength and damages in tension-leg platform hulls after a collision," *Ocean Eng.*, **286** 115668 (2023), doi: 10.1016/j.oceaneng.2023.115668.
44) A.M. Naufal, A.R. Prabowo, T. Muttaqie, H.I. Akbar, and D.F. Smaradhana, "Characterization of sandwich materials – Nomex-Aramid carbon fiber performances under mechanical loadings: Nonlinear FE and convergence studies," *Rev. Adv. Mater. Sci.*, **63** (*1*) 20230177 (2024), doi: 10.1515/rams-2023-0177.
45) S. Bansal, A. Tripathi, N. Kumar, T. Singh, and Ranganath M.S, "Modeling and analysis of finger splint for mild to high-grade mallet finger fracture," *Evergreen*, **10** (*2*) 1074–1079 (2023). doi:10.5109/6793665.
46) A.P. Fuadi, T. Muttaqie, A.C.P.T. Nugroho, Y.F. Kusuma, S. Mukti, M.A. Kurniawan, T. Firmandha, and M. Ismail, "Patrol Boat Strengthening Against a Collision with COLL Notation Based on Class Rules and Regulation in Indonesia – An Overview," *Mekanika: Majalah Ilmiah Mekanika*, **23** (*1*) 1-11 (2024), doi: 10.20961/mekanika.v23i1.74967.
47) I.B. Wiranto, S.O. Saraswati, I.R. Alfikri, C. Chairunnisa, F.C. Megawanto, M.I. Adhynugraha, and N.C. Majid, "Effect of Boundary Condition on Numerical Study of UAV Composite Skin Panels Under Dynamic Impact Loading," *Mekanika: Majalah Ilmiah Mekanika*, **23** (*1*) 22-32 (2024), doi: 10.20961/mekanika.v23i1.77875.
48) A.R. Prabowo, R. Ridwam, T. Tuswan, D.F. Smaradhana, B. Cao, and S.J. Baek, " Crushing resistance on the metal-based plate under impact loading: A systematic study on the indenter radius influence in grounding accident," *Appl. Eng. Sci.*, **18** 100177 (2024), doi: 10.1016/j.apples.2024.100177.
49) R. Ridwan, S. Sudarno, H. Nubli, A. Chasan, I. Istanto, and P.S. Pratama, Numerical Analysis of Openings in Stiffeners under Impact Loading: Investigating Structural Response and Failure Behavior, *Mekanika: Majalah Ilmiah Mekanika*, **22** (*2*) 115-125 (2023), doi: 10.20961/ mekanika.v22i2.76774.